Electronic Supplementary Material (ESI) for Lab on a Chip.

Supporting Information

Electrically controlled mass transport into microfluidic droplets from nanodroplet carriers with application in controlled nanoparticle flow synthesis

Tonghan Gu[a], Zheng Cao[a], Fan He[a], Yunfei Zhang[a], Saif A. Khan[b], and T. Alan Hatton[a*]

[a]Department of Chemical Engineering, Massachusetts Institute of Technology, 77 Massachusetts Avenue, Cambridge, MA 02139, USA. E-mail: tahatton@mit.edu.

[b]National University of Singapore, Department of Chemical and Bimolecular Engineering, 4 Engineering Drive 4 E5-02-28, 117576 Singapore. E-mail: saifkhan@nus.edu.sg.

Simulation of the convection-controlled scenario

The numerical simulation was conducted in COMSOL Multiphysics using a 3-D geometry. Under different flow rates, the volumes of the microdroplet plugs were calculated based on the flow rates and the measured microdroplet generation frequencies, which were 6.3 ± 0.3s, 2.8 ± 0.3s, and 0.87 ± 0.04s for 1x, 2x, and 5x multiples of the base flow rates (base CP: 50 μL/min and base DP: 10 μL/min) with a fixed CP to DP ratio of 5 to 1. From the values of droplet volumes, we computed microdroplet sizes based on the lubrication layer thickness obtained from equation (1), and the assumption that each microdroplet plug has two hemispherical ends (i.e. droplets do not wet the FEP tubing) and a cylindrical middle section. Although microdroplets kept expanding during electrocoalescence and eventually doubled their volumes, it was computationally too expensive to re-define the geometry and re-mesh a 3-D structure at every single time step. Thus,

we used 150% of the originally generated microdroplet volume, i.e. the average volume (since the final volume is 200% of the original volume), for simulation. A cross-sectional view of the geometry fed into COMSOL is schematically depicted in Figure S1 and the parameters are shown in Table S1 for three different flow rate conditions. A periodic boundary condition was imposed on the left (outlet) and the right (inlet) and a no-slip boundary condition was imposed on the tube inner surface. A slip boundary condition was used between the dispersed and the continuous phase. In this simulation, the frame of reference was fixed on the microdroplet and thus the velocity of the fluid was treated as a wall movement imposed on the no-slip tube inner surface. Brownian motion of the nanodroplets was treated with a diffusivity coefficient of 10^{-12} m/s calculated from the Stokes-Einstein relationship.

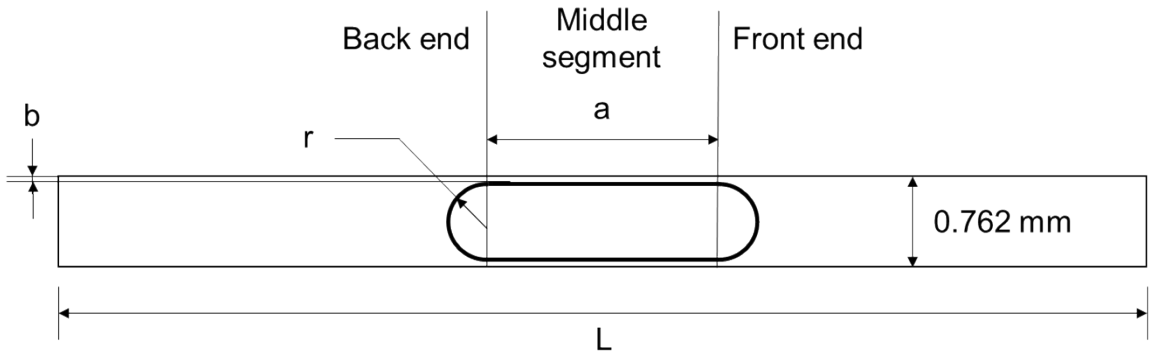

Figure S1. Cross-sectional view of the microdroplet plug dimension.

Table S1. Simulation geometries for different flow conditions

	b (mm)	L (mm)	a (mm)	r (mm)	volume (μL)	velocity (mm/s)
CP=50 μL/min DP=10 μL/min	0.013	13.8	3.05	0.368	1.05	2.2
CP=100 μL/min DP=20 μL/min	0.021	12.3	2.96	0.360	0.93	4.4
CP=250 μL/min DP=50 μL/min	0.036	9.5	2.45	0.345	0.725	11.0

The convection-controlled scenario can be achieved when the electrical field is sufficiently high. Under such a condition, electrocoalescence becomes very fast compared to the convective transport that brings nanodroplets from remote locations to the microdroplet surface. When we assume the electrocoalescence to be fast, we can neglect the fluid drag force near the microdroplet surface and only electrostatic force is significant. We separate an elongated microdroplet in three segments, the front end, the back end, and the middle segment, as shown in Figure S1. Considering the front end, from the *r*- and θ-directional interaction equations (2) and (3) in the main text, it can be derived that any nanodroplet located within the following limiting curved plane (as defined in the spherical coordinate in Figure 6)

$$r_{limit} = 1150 sin\theta \sqrt{cos\theta}\ [\mu m], \tag{S1}$$

will be consumed by the microdroplet eventually. A schematic illustration of the intersection between this curved plane and the cross-sectional plane (defined by Figure S1) is shown as red dotted lines in Figure S2. This curve is only slightly deviated from the straight connection line shown as blue solid lines in Figure S2. For simplicity, we use these solid straight lines in place of the dotted curved lines as the limiting boundary. The same limiting plane can also be defined symmetrically for the back end of the microdroplet. Note the equation is independent of ϕ and thus corresponds to a conical plane that is axisymmetric around the $\theta = 0$ vector. In the middle segment, the attractive zone could also be defined in a similar way considering this segment as a cylinder polarized by the electrical field. The 3-D structure of the enclosed region where electrostatic force is attractive is shown in Figure S3 (a). Since nanodroplets are also confined by the tubing inner surface, the actual feasible zone is limited, as shown in Figure S3 (b).

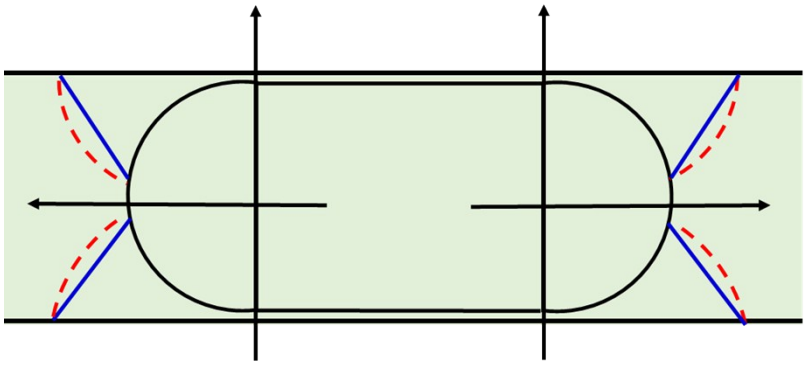

Figure S2. A schematic illustration of the intersection lines (red) and their approximation (blue) between the curved limiting plane defined by equation S1 and the cross-sectional plane.

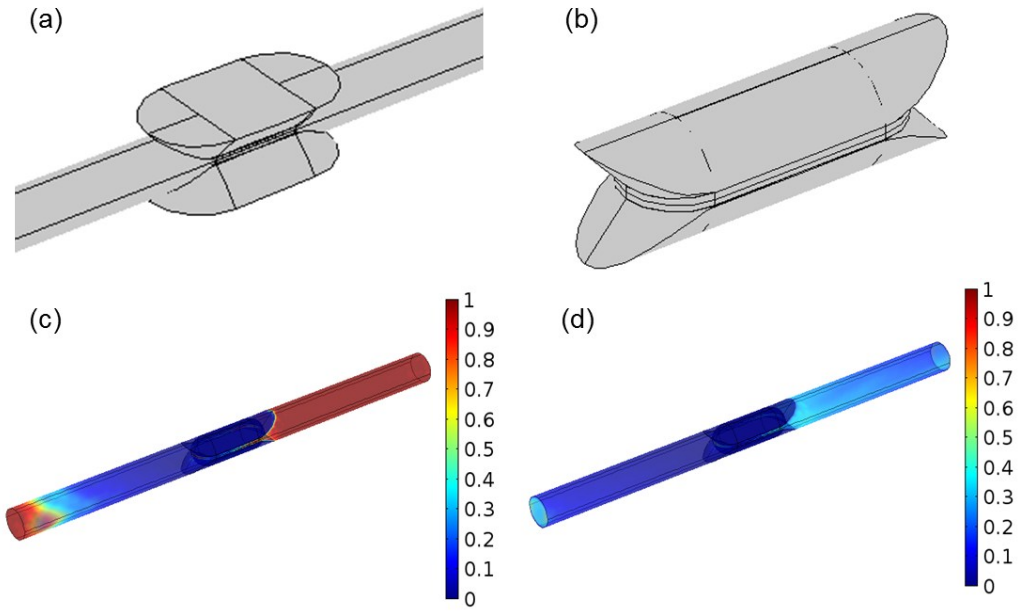

Figure S3 (a) A schematic of the limiting plane. (b) The intersection region (feasible zone) between the limiting plane and the tube inner wall constraint. The nanodroplet "concentration" distribution (c) 2s and (d) 10s after electrocoalescence begins for the flow condition of CP=50 μL/min, DP=10 μL/min.

Since electrostatic forces follow a fourth power decay with distance between the droplets, the electrostatic force is significantly less important compared to the fluid drag force when the nanodroplets are far from the microdroplet. For simplicity, we consider only fluid drag force outside the enclosed attractive zone defined in Figure S3 (b) but no electrostatic forces, which essentially converts this fourth power decaying force field into a sharp boundary where the electrostatic force is strong inside the attractive region but negligible outside. Under this assumption, we can treat nanodroplets as a chemical species with an initial "concentration" of unity, which undergoes a fast consumption reaction within the attractive region defined by the limiting plane and the tube inner wall constraint, as depicted in Figure S3 (b). Nanodroplet "concentration" quickly drops as the consumption starts, and the "concentration distribution" at two sampled time points is shown in Figure S3 (c) and (d). Nanodroplet "concentration" is then averaged over the entire continuous phase volume and converted to the fraction of remaining nanodroplets, which are compared to the experimental results in Figure 7(a).

Experimental set-up

As shown in Figure S4, the experimental set-up has six components, syringe pumps, function generator, waveform generator, amplifier, T-shaped fluid junction, and the home-made electrode assembly. The function generator and waveform generator are used to generate different signals to feed to the amplifier. The amplifier amplifies the voltage and supplies it to the electrodes, which comprise of a transparent ITO glass electrode on the top for visualization purpose, a copper sheet electrode on the bottom, and an acrylic spacer with slots for inserting tubings. When multiple injections are necessary, more syringe pumps are needed and each electrocoalescence process can be achieved by routing the tubing into one of the slots. A larger copper sheet replaces the ITO glass to cover all used slots.

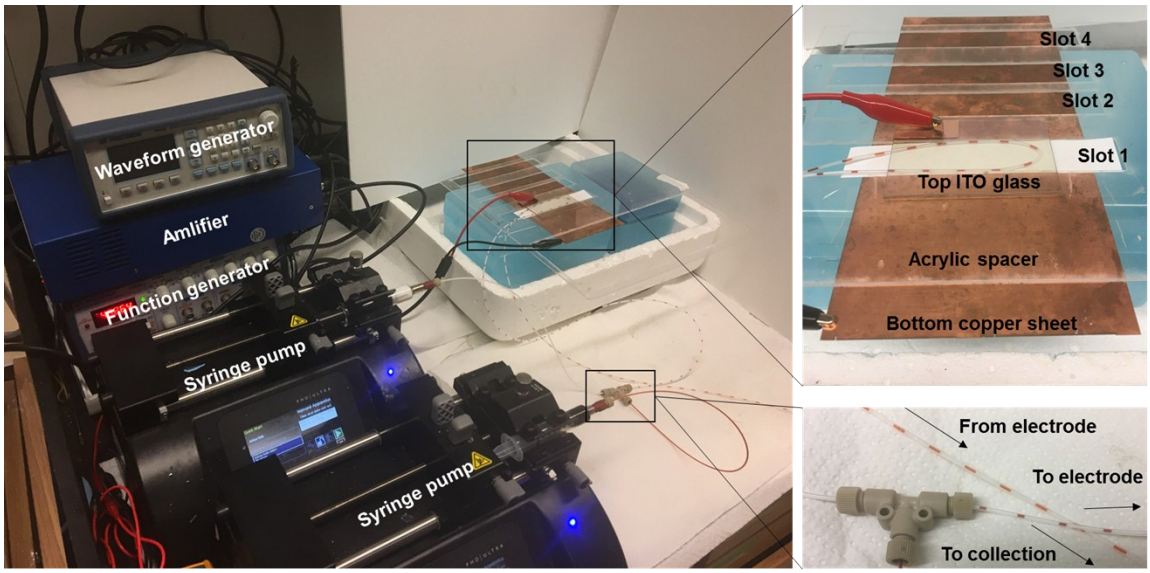

Figure S4. Experimental set-up and a zoom-in view of the 3-layer electrocoalescence assembly. We also show a comparison of the droplet size before and after electrocoalescence near the T-junction.

TEM images of gold nanoparticles prepared from different dosages of ascorbic acid

The TEM images and the associated histograms are presented in Figure S5. The mean diameters for samples prepared with 0.005 mM, 0.01 mM, and 0.02 mM of ascorbic acid and 0.01 mM of chloroauric acid are 26.1 ± 15.7 nm, 47.4 ± 15.0 nm, and 53.4 ± 12.2 nm. Note that even though the last sample (0.02 mM ascorbic acid and 0.01 mM chloroauric acid) comes from a molar reaction stoichiometry of two (ascorbic acid) to one (chloroauric acid), the maximum stoichiometry is 1.5 to 1 according to the reaction chemistry. Thus, the ascorbic acid is in excess. Figure S5(e) also shows that the particles are less spherical with protrusions along the peripheral.

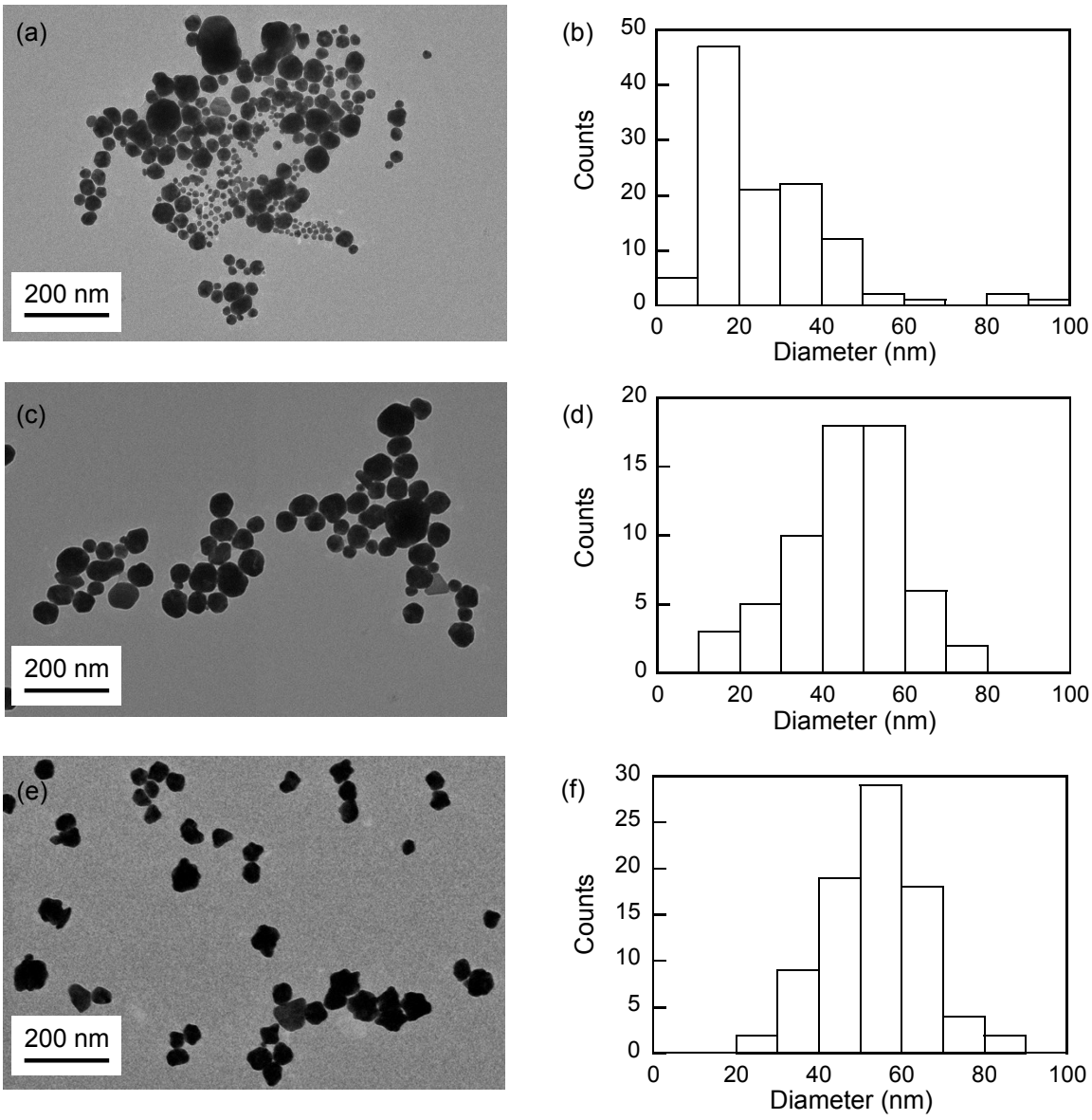

Figure S5. TEM images and size distribution histograms of gold nanoparticles prepared with (a) and (b) 0.005 mM ascorbic acid and 0.01 mM chloroauric acid, (c) and (d) 0.01 mM ascorbic acid and 0.01 mM chloroauric acid, and (e) and (f) 0.02 mM ascorbic acid and 0.01 mM chloroauric acid. All electrocoalescence processes were carried out under a high field of 11400 V/cm